A Nonlinear Circuit Simulation of Switching Process in Resonant-Tunneling Diodes

W-D. Zhang, *Senior, IEEE*, E. R. Brown, *Fellow, IEEE*, T. A. Growden, P. R. Berger, *Fellow, IEEE*, and R. Droopad, *Fellow, IEEE*

***Abstract*— A large-signal circuit model is used to compute the switching time for double-barrier resonant-tunneling diodes. The model consists of linear circuit elements plus a nonlinear *I–V* characteristic. The linear elements include a series resistor, a capacitor, and an inductor. The capacitance considers the charge accumulation, depletion in spacer layers, as well as charging-discharging of the quantum-well (QW) region. The inductance accounts for the delay of the current with respect to the voltage across the QW during the abrupt switching transition through the negative differential resistance region. A second-order Runge–Kutta method is used to solve for the switching transient, and then fit to experimental data for a high-quality InGaAs/AlAs resonant tunneling diode (RTD) using the QW inductance as a fitting parameter. Excellent agreement is found for the 10%–90% switching time with a calculated capacitance of 98 fF and a fitted inductance of 1300 pH. This large-signal inductance is approximately 7× greater than the small-signal inductance that has been successfully used to predict the fmax of RTDs such as the one tested here.**

***Index Terms*— Large signal, measurement, modeling, resonant tunneling diode (RTD), switching-time constant.**

I. Introduction

ELECTRON tunneling through potential-energy barriers in semiconductor heterostructures is a fast process as its transit time can be 100 fs or less. In addition, such tunneling can support high-speed, negative differential resistance (NDR) as first described in the pioneering work of Tsu and Esaki [1] and Chang *et al.* [2]. The NDR occurs as the lowest occupied energy levels in the emitter region drop in energy below the quasi-bound states of the heterostructure under external bias. This is the famous resonant-tunneling process, and its N-type *I–V* characteristic can be utilized for high-frequency self-oscillation and fast switching. Among tunneling devices, the double-barrier resonant-tunneling diode (RTD) is the most extensively studied NDR device. Waveguide-based RTD oscillations up to 712 GHz were demonstrated in the early 1990s [3], and then extended up to 1.1 THz by planar-circuit resonator techniques [4]. More recently, the oscillation frequency has been extended to ∼1.5 THz and beyond with efficient antenna coupling and electronic frequency tuning [5]–[7], providing a rejuvenated interest in resonant-tunneling devices. The justification for such high-frequency oscillations is provided by small-signal, lumped-element circuit theory and the popular concept of maximum frequency of oscillation, or $f_{\max}$ [3]. The lumped small-signal model is often extended to RTD switch circuit design. However, the switching behavior of RTDs necessarily involves a large-signal behavior not directly explicable by the small-signal model.

In [8], we reported fabrication and high-speed characterization of an InGaAs/AlAs double-barrier RTD. Its 10%–90% switching time was found to be 22 ps—significantly greater than the estimated large-signal *RC* switching time of 14.5 ps. Much of the discrepancy was attributed to the quantum-well (QW) lifetime τ_{QW}, which is 5.5 ps estimated from the Breit–Wigner approximation for transmission probability. However, this simple addition of characteristic times should be examined more carefully, since the physical effects that determine the current density and NDR, such as the barrier thickness, also influence the QW lifetime. So a better approach is to estimate the switching time with a large-signal circuit model in which nonlinear R, C, and L are all coupled through instantaneous circuit action. In this paper, we carry out such a calculation and test it against the experimental results for the same high-quality InGaAs/AlAs RTD. Previously, the large-signal model was developed for RTDs [9], [10], but has never been tested by switching measurements.

This paper is organized as follows. Section II presents a brief introduction of our RTD device and switching-time measurements. Section III constructs the large-signal circuit model for RTDs. Section IV compares the modeling results to experimental data. Section V presents the conclusion.

II. Measurements

The RTD device under test was grown by molecular-beam epitaxy as an InGaAs/AlAs heterostructure on a semi-insulating InP substrate. Its active region is comprised of two unintentionally doped AlAs barriers (thickness = 2.4 nm) separated by an undoped In0.53Ga0.47As QW (width = 4.4 nm) layer (Fig. 1). Details on device fabrication can be found in [8]. The switching setup is shown in Fig. 2(a). The ramp signal consists of a dc offset V_0 and a triangular wave $V_R = V_0 + V_T(t)$, and is fed into one port of the bias tee.

Manuscript received April 1, 2016; revised July 11, 2016 and October 2, 2016; accepted October 3, 2016. Date of publication October 28, 2016; date of current version November 22, 2016. This work was supported by the Office of Naval Research MURI Program under Award N00014-11-1-0721. The review of this paper was arranged by Editor A. J. Scholten.

W-D. Zhang and E. R. Brown are with Departments of Physics and Electrical Engineering, Wright State University, Dayton, OH 45435 USA (e-mail: wzzhang@fastmail.fm; elliott.brown@wright.edu).

T. A. Growden and P. R. Berger are with The Ohio State University, Columbus, OH 43210 USA.

R. Droopad is with Department of Physics, Texas State University, San Marcos, TX 78666 USA.

Color versions of one or more of the figures in this paper are available online at http://ieeexplore.ieee.org.

Digital Object Identifier 10.1109/TED.2016.2617681

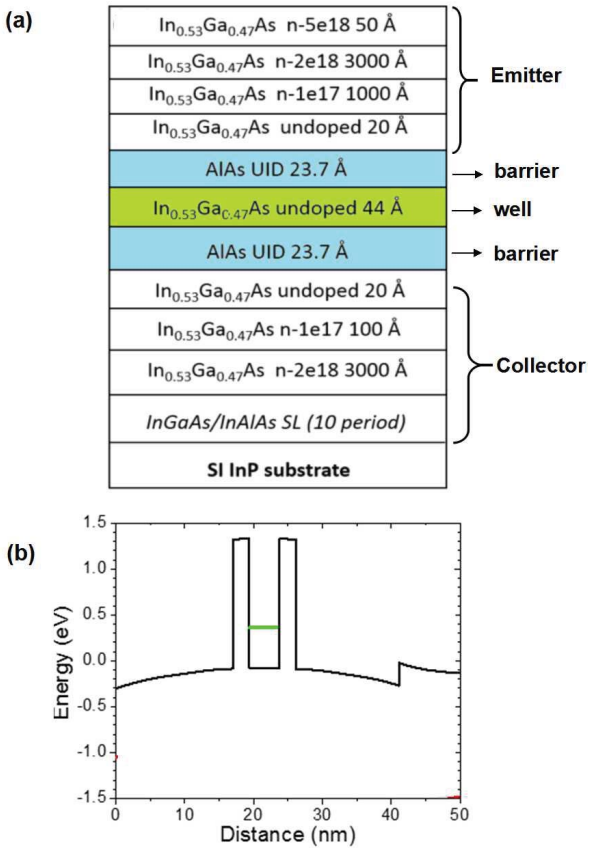

Fig. 1. (a) Epitaxial layer structure for the RTD. (b) Band structure showing the first quasi-bound level [8].

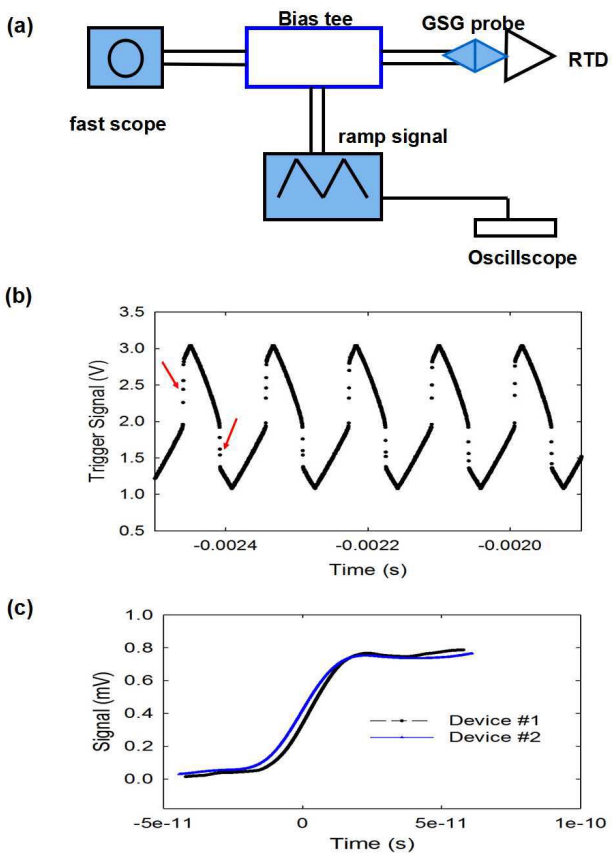

Fig. 2. (a) Switching-time measurement setup. (b) Ramp signal monitored with the slow-speed oscilloscope. Red arrows mark the peak-to-valley (the left arrow)and valley-to-peak (the right arrow) switching events, respectively. (c) Peak-to-valley switching waveform measured with the fast-speed scope.

The repetition frequency of the triangular wave $V_T(t)$ is set to 8.6 or 86 kHz, and no significant influence on switching time is found. The second port of the bias tee is connected to a GSG probe, which contacts the coplanar-waveguide pad of the RTD during test. V_0 and $V_T(t)$ are properly adjusted, such that a switching transient is triggered. The switching waveform is coupled from the output port of the bias tee to a real-time Tektronix MS073304DX oscilloscope, which has a risetime of $\tau_o = 13$ ps for the instrumental settings used. Shown in Fig. 2(b) is the switching as monitored on a slow oscilloscope through the bias port. The peak-to-valley and valley-to-peak switching events are represented by the precipitous black-dotted line segments denoted with red arrows. A typical switching event obtained with the fast scope is shown in Fig. 2(c). The 10%–90% risetime is estimated to be $\tau_m = 25.3$ ps from the measured curve, and the extracted "intrinsic" 10%–90% risetime is $\tau_s = 21.7$ ps after accounting for the fast scope risetime τ_o from τ_m with $\tau_s = (\tau_m^2 - \tau_o^2)^{1/2}$ [8].

To test the consistency of the experimental method, a second device is tested. It is fabricated from the same wafer as the first one, and displays practically the same NDR characteristics. Measurement of the 10%–90% switching time yields 19.9 ps [Fig. 2(c)].

The testing of four more devices yields a mean switching time 22.3 ps and a standard deviation 2.9 ps. Whether the 2.9 ps deviation is due to measurement uncertainty or device-to-device variation is still not clear.

III. Modeling

To simulate the switching event, we develop a large-signal model, which includes both QW capacitance and inductance, as shown in Fig. 3(a). The physics behind each element is explained as follows. R_s is the series resistance in the flat-band semiconductor outside the active device region. C_r is the capacitance contributed by the electron accumulation in the emitter region, depletion in the collector-region, and charging–discharging of the QW region (Fig. 1). L_s is the inductance to account for the lag of the current behind the steep voltage variation during switching through the NDR region. R_L is the load resistance assuming that any load reactance is insignificant.

From Kirchhoff's laws, we can write two differential equations for the voltage across the capacitor $V_C(t)$ and the current flow through the RTD resistive branch $I_D(t)$

$$C_r \frac{dV_C(t)}{dt} = \frac{[V_R(t) - V_C(t)]}{(R_L + R_s)} - I_D(t) \tag{1}$$

$$L_s \frac{dI_D(t)}{dt} = V_C(t) - V_D(t) \tag{2}$$

where $V_D(t)$ is a function of $I_D(t)$ or vice versa, and the switching signal is calculated with

$$V_s(t) = V_C(t) + \left[I_D(t) + C_r \frac{dV_C(t)}{dt} \right] R_s. \tag{3}$$

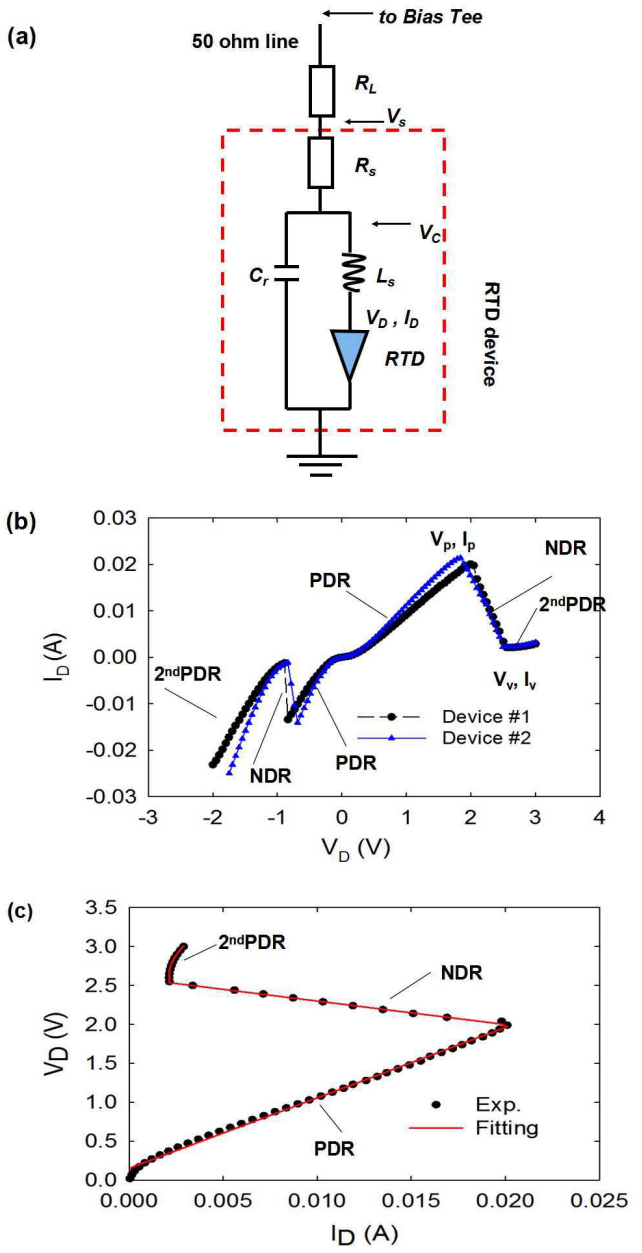

Fig. 3. (a) Large-signal model for RTD. (b) Experimental I–V curve of RTD (device 1). (c) Voltage–current curve (forward) and its piecewise fitting functions in PDR, NDR, and the second-PDR regions.

Equations (1)–(3) are similar to the small-signal lumped-circuit model used previously for oscillator $f_{\max}$ analysis [3]. The difference is that the relation between the current I_D and the bias voltage V_D is replaced by the experimental dc I–V curve.

A typical I–V curve in both forward and reverse directions is shown in Fig. 3(b) (device #1). The sweeps go from low to high. Both NDR regions are associated with the lowest quasi-bound level within the QW of the RTD. As the voltage is increased beyond the valley at negative or positive bias, the conduction enters a second-PDR region, which is related to either the second resonant level or inelastic tunneling (leakage) through the first level. Device #2 has almost identical I–V characteristics.

Next, the relationship $V_D(t) = V_D[I_D(t)]$ needs to be established, which is necessary to implement a numerical Runge–Kutta method. Although, in principle, the experimental I–V curve can be implemented into computer programming through a direct table search-interpolation scheme, an analytic solution is desirable, because it significantly reduces the computation time. When the bias is in the (first) PDR region ($0 < V_D < V_P$), the I–V curve is approximated with

$$V_D(t) \approx R_{Dp} I_D(t) + V_{\text{ot}} \tag{4}$$

where R_{Dp} is the resistance in the positive differential resistance region, and V_{ot} is the offset voltage. When V_D is in the NDR region ($V_P \le V_D \le V_V$), the I–V curve is approximated by

$$V_D(t) \approx R_{Dn} I_D(t) + V_V \tag{5}$$

where R_{Dn} is the negative resistance in the NDR region, and V_V is the voltage at the valley. The voltage–current relation in the second-PDR region ($V > V_V$) can be approximated by

$$V_D(t) \approx \sqrt{[I_D(t) - I_V]/B} + V_V \tag{6}$$

where B is a curve coefficient and I_V is the valley current.

Note that the linear behavior displayed in the NDR region of Fig. 3(c) is likely a result of switching, not the natural I–V curve in the NDR region. If this is the case, (5) can be replaced with

$$V_D(t) \approx V_V - \sqrt{[I_D(t) - I_V]/B}. \tag{7}$$

The parameters are obtained from Fig. 3(b): $V_P = 1.99$ V, $V_V = 2.60$ V, $I_V = 2.1$ mA, $R_{Dp} \sim 90.9$ Ohm, $R_{Dn} \sim 30.1$ Ohm, $V_{\text{ot}} = 0.152$ V, and $B = 0.0048$ A/V^2. With these parameters, the fitting curve on current–voltage relationship is shown in Fig. 3(c), showing excellent agreement with the experiment one.

Furthermore, the series resistance R_s is estimated to be ~3 Ohm [3]; the resistance $R_L = 50$ Ohm is the SMA characteristic impedance. The capacitance C_r is obtained from numerical computations of band-bending using the BandProf software tool [11]. This yields a value of 1.8 fF/μm^2 at the peak voltage of ~2.0 V. The device active area is 6×9 μm^2, so the capacitance is $C_r \sim 98$ fF. The value of L_s will be extracted from experimental data instead of being calculated from first principle consistent with the large-signal modeling goal of this paper.

Finally, the initial conditions for the differential equations (1) and (2) are $V_C(t = 0) = V_0 R_{Dp}/(R_{Dp} + R_L + R_s)$, and $I_D(t = 0) = V_0/(R_{Dp} + R_L + R_s)$. And $V_C(t)$ and $I_D(t)$ are required to be continuous in all regions of the RTD operating curve.

IV. Results and Discussion

The nonlinear differential equations are solved numerically with the second-order Runge–Kutta method [12]. In the simulation, we choose the frequency of the ramp signal to be 640 MHz, which is much higher than the ramp frequencies 8.6 and 86 kHz actually used in measurements. Such a high ramp frequency is used to reduce computation time, because a very fine step size is required in Runge–Kutta computation

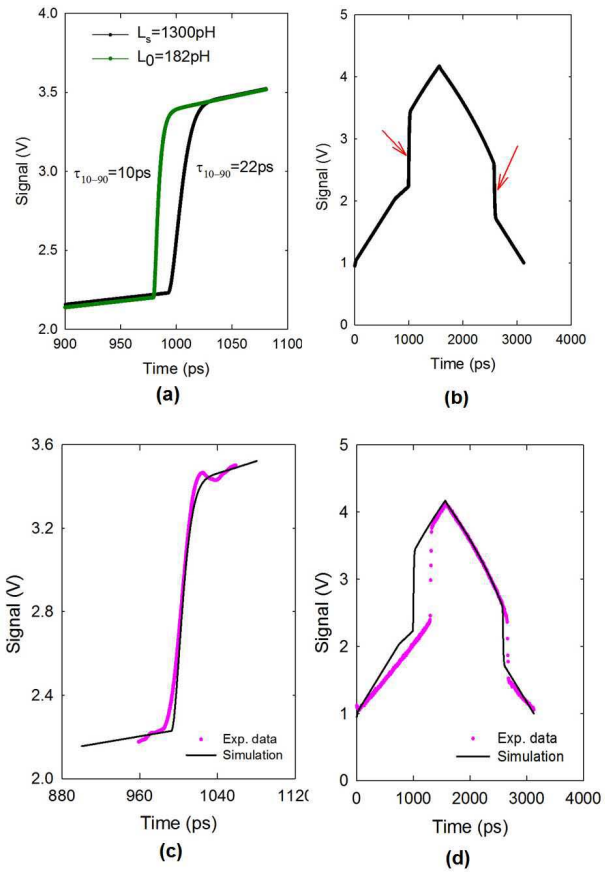

Fig. 4. Large-signal modeling results. (a) Switching process. (b) Peak-to-valley and valley-to peak switching events driven by one cycle of triangular ramp signal. (c) Overlay of the simulation result shown in (a) versus experimental data from Fig. 2(c). Note, to compare with the simulation, the experimental curve is necessarily transformed with translation and linear scaling as the ramp frequency used in the simulation is different from the experimental data. The comparison shows very good agreement between the experiment and the modeling. (d) Overlay of the simulation shown in (b) versus the experimental data from Fig. 2(b). To compare with the simulation, the experimental curve is necessarily transformed with translation and linear scaling.

in order to discern the ps-scale switching event. Whatever frequency used, however, should not change the results and conclusions reached by the numerical simulations. The dc offset of the ramp signal is set at $V_0 = 1.5$ V, and the amplitude of the triangular wave is 4.9 V.

We estimate $L_s \sim 1300$ pH, which together with the capacitance ~98 fF yields a 10%–90% switching time of $\tau_s = 22$ ps. The switching curve is calculated and shown in Fig. 4(a), and it almost reproduces exactly the experimental one obtained with fast oscilloscope shown in Fig. 2(c) [Fig. 4(c)]. Furthermore, we are able to generate both peak-to-valley and valley-to-peak switching processes within a cycle of the ramp signal, as shown in Fig. 4(b). This curve agrees well qualitatively with the experimental data obtained with the low-speed oscilloscope in Fig. 2(b) [Fig. 4(d)]. Note that the simulated curve in Fig. 4(b) shows that the nearly vertical peak-to-valley transition (indicated by the left red arrow) is positioned higher than the valley-to-peak transition (right red arrow) as observed in the experimental ramp-signal curve of Fig. 2(b).

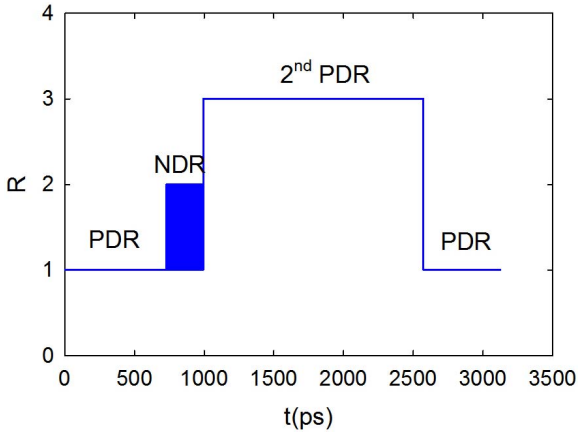

Fig. 5. Operational stages of the RTD device during a cycle of ramp signal determined by calculating the bias voltage of RTD, V_D. If device operates in PDR region, then R is set as 1; if in NDR region, R is set as 2; and if in the second-PDR region, R set as 3. Note the shaded area of the NDR region indicates the oscillation of V_D between the PDR and NDR regions.

In the numerical simulation, the operating stage of the RTD is also recorded and shown in Fig. 5, which has the same ramp-signal cycle as Fig. 4. Here, if the device operates in the PDR region ($0 < V_D < V_P$), then the R value is set as 1; if in the NDR region ($V_P \leq V_D \leq V_V$), R is set as 2, and if in the second-PDR region($V > V_V$), R set as 3. As the bias ramps up from V_0, the RTD initially operates in the PDR, and then moves across into the NDR region, which is noticeably unstable-oscillating back and forth between the PDR and the NDR. The peak-to-valley switching occurs when the RTD transits from the oscillating NDR to the second-PDR region, while the valley-to-peak switching occurs as the RTD transits from the second PDR to the first PDR region. Therefore, the switching behaviors must involve the second-PDR region, which is contributed by either tunneling from the second quasi-bound level or inelastic current (leakage) through the ground level.

We found out that the amplitude of the ramp signal has a negligible effect on the switching time τ_s. For example, τ_s changes from 22.0 to ~21.3 ps as the amplitude V_T changes from 4.9 to 4.0 V. The series resistance also has a little effect on the switching time: τ_s changes from 22.0 to 21.5 ps as R_s changes from 3 to 10 Ohm. These are as expected, since intuitively L_s, C_r and the nonlinear I–V characteristic of the RTD should be the major factors in determining large-signal switching speed.

In previous work on sinusoidal oscillators, the inductance L_0 was found proportional to a time constant divided by mean differential conductance, $L_0 = \tau_N / g_D$ [13], [14]. The time constant τ_N was the time taken in order for the device to reestablish a new steady state as its bias voltage is rapidly switched from V_D to $V_D + \Delta V$. The mean NDR conductance (small signal) is evaluated as 30.3 mS in Fig. 3(b), and the theoretical QW lifetime $\tau_{QW} \sim 5.5$ ps is estimated with the Breit–Wigner equation. The inductance is then estimated $L_0 = \tau_N / g_D \sim 182$ pH, which is significantly (~7 times) smaller than the value obtained with the present large-signal model [Fig. 4(a)]. This inconsistency indicates the large-signal response time for the device to reestablish a new steady state

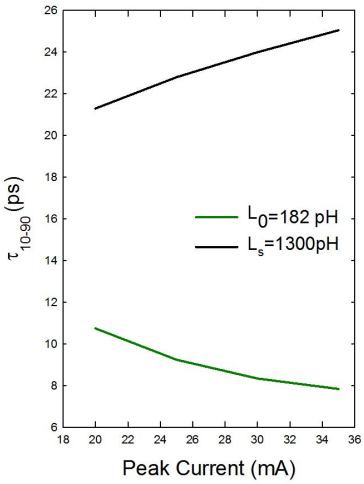

Fig. 6. Influence of peak current on switching time simulated with the large-signal model.

can be longer than the QW lifetime during a switching event because of the involvement of the conducting transition from the NDR to the second-PDR region.

The effect of peak current I_P on switching time τ_s is studied with the large-signal model. When the inductance $L = L_0$ is small, simulations indicate that RTD switching time can be reduced by increasing peak current, while the rest of parameters are kept the same. This is consistent with the RC model, which predicts $t_R \sim 4.4C_rV_D/(I_P - I_V)$. However, when the inductance $L = L_s$ is large, simulations predict the switching time increases as the peak current increases (Fig. 6). Hence, large-signal inductance needs to be minimized for optimized high-speed operation. This can be achieved by reducing the thickness of barriers and the portion of the second-PDR current from the leakage of the ground level.

V. Conclusion

A large-signal numerical simulation has been made of an RTD undergoing switching across the NDR region, and comparison is made with experimental switching results for an InGaAs/AlAs double-barrier device. The large-signal circuit model includes linear capacitance, inductance, and series resistance elements, and a piecewise linear I–V characteristic. The switching behavior is solved in the time domain by the second-order Runge Kutta. Through a curve-fitting procedure with the one free-parameter L, we find an excellent agreement with experiment for a large-signal value of L approximately $7\times$ larger than the small-signal inductance used for small-signal ($f_{\max}$) calculations.

References

[1] R. Tsu and L. Esaki, "Tunneling in a finite superlattice," *Appl. Phys. Lett.*, vol. 22, no. 11, p. 562, 1973.
[2] L. L. Chang, L. Esaki, and R. Tsu, "Resonant tunneling in semiconductor double barriers," *Appl. Phys. Lett.*, vol. 24, no. 12, p. 593, 1974.
[3] E. R. Brown, J. R. Söderström, C. D. Parker, L. J. Mahoney, K. M. Molvar, and T. C. McGill, "Oscillations up to 712 GHz in InAs/AlSb resonant-tunneling diodes," *Appl. Phys. Lett.*, vol. 58, no. 20, p. 2291, 1991.
[4] M. Feiginov, C. Sydlo, O. Cojocari, and P. Meissner, "Resonant-tunnelling-diode oscillators operating at frequencies above 1.1-THz," *Appl. Phys. Lett.*, vol. 99, no. 23, p. 233506, Dec. 2011.
[5] M. Feiginov, H. Kanaya, S. Suzuki, and M. Asada, "Operation of resonant-tunneling diodes with strong back injection from the collector at frequencies up to 1.46 THz," *Appl. Phys. Lett.*, vol. 104, no. 24, p. 243509, Jun. 2014.
[6] T. Maekawa, H. Kanaya, S. Suzuki, and M. Asada, "Frequency increase in terahertz oscillation of resonant tunnelling diode up to 1.55 THz by reduced slot-antenna length," *Electron. Lett.*, vol. 50, no. 17, pp. 1214–1216, Aug. 2014.
[7] S. Kitagawa, S. Suzuki, and M. Asada, "650-GHz Resonant-tunneling-diode VCO with wide tuning range using varactor diode," *IEEE Electron Device Lett.*, vol. 35, no. 12, pp. 1215–1217, Dec. 2014.
[8] T. A. Growden, E. R. Brown, W. Zhang, R. Droopad, and P. R. Berger, "Experimental determination of quantum-Well lifetime effect on large-signal resonant tunneling diode switching time," *Appl. Phys. Lett.*, vol. 107, no. 15, p. 153506, Oct. 2015.
[9] T. H. Kuo, H. C. Lin, U. Anandakrishnan, R. C. Potter, and D. Shupe, "Large-signal resonant tunneling diode model for SPICE3 simulation," in *Tech. Dig., Int. Electron Devices Meeting (IEDM)*, Dec. 1989, pp. 567–570.
[10] Z. Yan and M. J. Deen, "New RTD large-signal DC model suitable for PSPICE," *IEEE Trans. Comput.-Aided Des. Integr. Circuits Syst.*, vol. 14, no. 2, pp. 167–172, Feb. 1995.
[11] W. Frensley, *Bandprof Software*. Dallas, TX: Univ. of Texas Press, 2015.
[12] E. W. Weisstein. Runge-Kutta Method. From MathWorld—A Wolfram Web Resource. [Online]. Available: http://mathworld.wolfram.com/Runge-KuttaMethod.html
[13] N. G. Einspruch and W. R. Frensley, *Heterostructure and Quantum Devices*, ed. Orlando, FL: Academic, 1994, p. 306.
[14] E. R. Brown, C. D. Parker, and T. C. L. G. Sollner, "Effect of quasibound-state lifetime on the oscillation power of resonant tunneling diodes," *Appl. Phys. Lett.*, vol. 54, no. 10, p. 934, Jan. 1989.

W-D. Zhang (S'03–M'05) received his Ph.D degree in 2005 from University of Virginia.

He is a research physicist with Terahertz Sensors Lab of Wright State University. His research is focus on novel electric materials, semiconductor devices, submillimeter/terahertz sensing and medical imaging.

E. R. Brown (M'89–SM'95–F'00) received the Ph.D. degree in applied physics from the California Institute of Technology, Pasadena, CA, USA, in 1985.

He is currently a Professor of Electrical and Computer Engineering with the University of California at Santa Barbara, Santa Barbara, CA.

Dr. Brown has been a fellow of the American Physical Society since 2007. He was a recipient of the 1998 Outstanding Achievement Award from the U.S. Office of the Secretary of Defense.

T. A. Growden received the Ph.D. degree in electrical and computer engineering from The Ohio State University, Columbus, OH, USA, in 2016.

He is currently a Post-Doctoral Researcher in electrical engineering with The Ohio State University. His current research interests include design, fabrication, and characterization of Si and III-nitride-based tunneling devices.

Dr. Growden received an Honorable Discharge in 2005 and separated from the military as a Sergeant.

P. R. Berger (S'84–M'91–SM'97–F'11) received the Ph.D. degree in electrical engineering from the University of Michigan, Ann Arbor, MI, USA.

He is currently a Professor with The Ohio State University, Columbus, OH, USA. He is also a Distinguished Visiting Professor with the Tampere University of Technology, Tampere, Finland.

Dr. Berger was a recipient of the Outstanding Engineering Educator Award. He is an IEEE EDS Distinguished Lecturer. He is a Senior Member of OSA.

R. Droopad, photograph and biography not available at the time of publication.